Research Article Vol. 2, No. 4 / April 2015 / Optica 329

# High-fidelity visualization of formation of volume nanogratings in porous glass by femtosecond laser irradiation

Yang Liao,[1,†] Jielei Ni,[1,†] Lingling Qiao,[1] Min Huang,[2] Yves Bellouard,[3] Koji Sugioka,[4] and Ya Cheng[1,*]

[1]State Key Laboratory of High Field Laser Physics, Shanghai Institute of Optics and Fine Mechanics, Chinese Academy of Sciences, Shanghai 201800, China

[2]State Key Laboratory of Optoelectronic Materials and Technologies, Sun Yat-sen University, Guangzhou 510275, China

[3]Mechanical Engineering Department, Eindhoven University of Technology, 5600 MB Eindhoven, The Netherlands

[4]RIKEN-SIOM Joint Research Unit, RIKEN Advanced Science Institute, Center for Advanced Photonics, Hirosawa 2-1, Wako, Saitama 351-0198, Japan

*Corresponding author: ya.cheng@siom.ac.cn

Received 22 December 2014; revised 18 February 2015; accepted 19 February 2015 (Doc. ID 231316); published 30 March 2015

**Formation of self-organized nanogratings in bulk glasses with femtosecond laser pulses is one of the most intriguing phenomena in the interactions of light with transparent materials. With the feature sizes far beyond the optical diffraction limit, these nanostructures have found widespread applications in nanophotonics and nanofluidics. The physics of the phenomenon is still far from being fully understood, largely because of the lack of a technique for noninvasively visualizing the formation of the nanogratings embedded within bulk glasses. Here, we access the snapshots of morphologies in the laser-affected regions in a porous glass that reveal the evolution of the formation of nanogratings with an increasing number of laser pulses. Combined with further theoretical analyses, our observation provides important clues that suggest that excitation of standing plasma waves at the interfaces between areas modified and unmodified by the femtosecond laser irradiation plays a crucial role in promoting the growth of periodic nanogratings. The proposed universal nanostructure growth mechanism involving laser-induced plasma wave formation at the interfaces of the seed structures may tie together many previous observations, meanwhile linking the in-volume nanograting formation to previously discovered mechanisms for surface nanoripple formation.** 

***OCIS codes:*** (140.3390) Laser materials processing; (140.7090) Ultrafast lasers; (160.2750) Glass and other amorphous materials; (270.4180) Multiphoton processes; (220.4241) Nanostructure fabrication.

http://dx.doi.org/10.1364/OPTICA.2.000329

## 1. INTRODUCTION

Recently, the interaction of ultrafast laser pulses with condensed matter has attracted significant attention. It opens new horizons in strong field laser physics and attosecond science, which have largely focused on gaseous media over the past two decades, as well as new avenues for material laser processing beyond the diffraction limit (i.e., with nanoscale spatial resolutions) and with three-dimensional (3D) capabilities [1–3]. Specifically, irradiation of intense ultrafast laser pulses inside dielectric materials has led to intriguing phenomena, such as the formation of nanovoids and periodic nanogratings [4–7], glass constituent redistribution [8], nonreciprocal writing [9–11], and formation of new phases of matter [12]. Among them, the formation of nanogratings has been intensively investigated since its discovery, as the feature size of the nanograting is much less than the incident

irradiation wavelength, which provides promising potential for applications ranging from nanophotonics [13,14] to nanofluidics [15]. At present, several models have been proposed to explain this phenomenon, including interference between the incident light field and the electric field of the bulk electron plasma wave excited by the incident light [5], the formation of randomly distributed nanoplasmas due to the initial inhomogeneous multiphoton absorption in the focal volume, which self-organize into periodic nanoplanes [6], and very recently, the coupling between attractive interaction and self-trapping of exciton-polaritons [16]. Nevertheless, a convincing explanation that explains all reported experimental observations has not yet been proposed. For direct observation of nanogratings formed in glasses by either a scanning electron microscope (SEM) or atomic force microscope, the fabricated structures must be exposed to ambient air, typically by cleavage or focused ion beam milling [17]. Afterward, chemical wet etching is employed to facilitate the observation of nanogratings. This post-chemical-wet-etching process, however, can modify or even destroy some fine features in the laser-modified zones (LMZs) [18]. We show that porous glass, which has been employed for fabricating 3D microfluidic and nanofluidic devices [19,20], provides us an ideal platform for investigating the evolution of nanogratings during their formation, because the irradiation by an intense femtosecond laser of porous glass immersed in water can induce efficient ablation, resulting in the formation of periodic hollow nanocracks. As a result, the fine morphological features in the LMZ can be directly displayed under a SEM after cleavage of the prepared samples without the invasive chemical wet etching. The elimination of chemical wet etching is crucial for high-fidelity visualization of the formation of volume nanogratings. Therefore, the porous glass serves as an ideal 3D recording medium that allows us to access the high-fidelity snapshots during the formation of nanogratings. Based on our observation, we suggest that excitation of plasma waves at the interface between the areas modified and unmodified by femtosecond laser irradiation plays a crucial role in initiating the formation of nanogratings.

Despite the fact that the mechanism of nanograting formation by repeated femtosecond irradiation remains controversial, several nanotechnologies have already been established over the past few years [5,6,13–18,20–25]. By inscribing nanogratings in fused silica with controllable orientation angles in a space-selective manner, novel photonic devices including polarization-sensitive devices [13] and five-dimensional optical data storage [14] have been demonstrated. Inscription of isolated nanocracks in porous glass has also enabled the fabrication of nanofluidic channels with a width of ~40 nm, in which the analysis of single DNA molecules has been performed [15]. The deep understanding revealed by our findings will not only lead to enhancement of the performance of existing nanophotonic and nanofluidic devices but also foster innovative applications such as nanodroplet production, bioseparation at the nanoscale, and optical metamaterials.

## 2. EXPERIMENT

The schematic of our experimental setup is illustrated in Fig. 1. In our experiment, high-silicate porous glass samples were used as the substrates, which were produced by removing the borate phase from phase-separated alkali-borosilicate glass in a hot acid solution [26]. Details of the glass can be found elsewhere [20]. To induce the nanograting structures, a high-repetition regeneratively amplified Ti:sapphire laser (Coherent, Inc., RegA 9000) with a pulse duration of ~100 fs, a central wavelength of 800 nm, and a repetition rate of 250 kHz was used. The Gaussian laser beam with an initial 8.8 mm diameter was passed through a ~3 mm diameter aperture, i.e., only the central part of the laser beam was used because of its high homogeneity. A long-working-distance water-immersion objective (N.A. = 1.10) was employed for focusing the beam into the porous glass. The glass sample was fixed in a petri dish filled with distilled water.

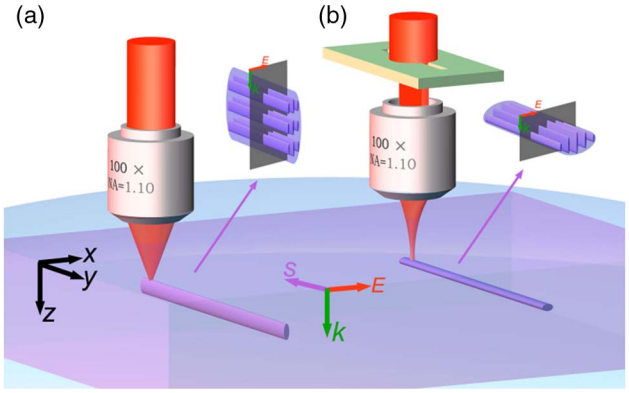


**Fig. 1.** Schematic illustrations of femtosecond laser direct writing setups (a) without and (b) with slit-beam shaping. Insets: close-up views of the nanogratings induced in the written tracks. The laser incident direction ($k$), polarization direction ($E$), and the writing direction ($S$) are indicated in the figure.

The femtosecond laser beam was focused in the volume of porous glass with two different focusing geometries. In the first geometry [Fig. 1(a)], the femtosecond laser beam was directly focused into the glass using the water-immersion objective, whereas in the second geometry [Fig. 1(b)], a narrow slit with a width of 0.6 mm and a length of 5 mm was placed above the objective lens, resulting in an expansion of the focal spot in the transverse direction. It is worth mentioning that since a water immersion objective was used in all the experiments, spherical aberration was practically eliminated in both the focusing geometries. The nanogratings formed in the tracks written with different focusing geometries are schematically illustrated in the insets of Fig. 1. The purpose of the slit is to increase the focal spot size in the transverse direction and reduce the interaction length of the femtosecond laser with the glass in the longitudinal direction [i.e., along the $Z$ axis as indicated in Fig. 1(a)] [27]. In all the experiments, the laser pulses were focused ~170 μm below the surfaces of the glass samples. To characterize the morphologies of the embedded nanogratings, the fabricated samples were cleaved (i.e., without further polish) along the plane perpendicular to the writing direction to access the cross sections of the LMZs. The revealed nanograting structures were directly characterized using a SEM (Zeiss Auriga 40).

Neither chemical etching nor annealing was used before the SEM examinations.

## 3. RESULTS AND DISCUSSION

First, we present SEM images of the cross sections of the nanostructures inscribed in the porous glass at a low pulse energy of 50 nJ and various scan velocities without the slit in Fig. 2. Under this laser intensity, an isolated subwavelength-width crack (SWC) with a transverse dimension of ~40 nm can be formed with a sufficient number of laser pulses [20]. At the highest scan velocity of 25 mm/s, which corresponds to the least number of laser pulses deposited in the focal volume, a nanovoid with a diameter of ~300 nm was formed in the central area of the focal spot [Fig. 2(a)]. By reducing the scan velocity to 10 mm/s, it is found that some defects, which appear under the SEM to be hollow nanovoids with diameters larger than those of the original nanopores, started to gather along the optical axis of the incident laser in its backward direction, as indicated by the white arrows in Figs. 2(b) and 2(c). Further reduction of the scan velocity leads to the formation of a mature SWC, as shown in Figs. 2(d) and 2(e). The growth of the single SWC occurs in both the backward and forward directions, as shown in Fig. 2(e).

When the pulse energy was increased to 120 nJ, which is well above the ablation threshold, we found that the induced phenomena are completely different from those in Fig. 2. At the beginning, a well defined LMZ can be formed around the focus, in which a large number of randomly distributed defects are formed [Fig. 3(a)]. It should be stressed that at this stage, there is not any signature of nanograting formation in the LMZ. With an increasing number of pulses, it is clear that due to the modified optical property around the LMZ, the nonlinear propagation of the laser pulses leads to more complex behaviors such as single and multiple self-refocusing, as shown in Figs. 3(b)–3(d), respectively. Interestingly, after a certain number of laser pulses, some signature of a periodically arranged nanovoid array appears in Figs. 3(d) and 3(e). A close examination reveals that the periodic nanovoid chain is preferentially formed at the interface between the regions modified and unmodified by the femtosecond laser irradiation, as indicated by the black arrows in Figs. 3(d) and 3(e). Finally, after irradiation with more laser pulses, the nanovoids in Fig. 3(e) all grow into SWCs aligned in parallel with the laser propagation

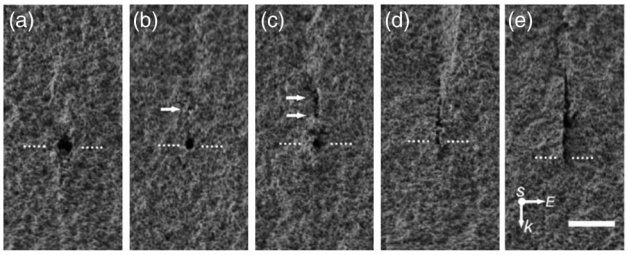


**Fig. 2.** Evolution from a single nanovoid to a nanocrack. Scan velocities in (a)–(e) are 25, 10, 5, 2.5, and 1 mm/s, respectively. Scale bar: 1 μm. Position of the focal point is indicated by the dashed lines in each panel. The laser incident direction ($k$), polarization direction ($E$), and the writing direction ($S$) are indicated in the figure.

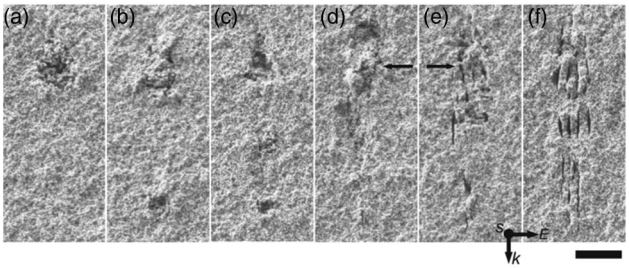


**Fig. 3.** Cross-sectional morphologies of nanogratings written without slit-beam shaping. Scan velocities in (a)–(f) are 30, 25, 15, 5, 1, and 0.95 mm/s, respectively. Scale bar: 1 μm. The laser incident direction ($k$), polarization direction ($E$), and the writing direction ($S$) are indicated in the figure.

direction, leading to the formation of a periodic nanocrack array (PNCA), as shown in Fig. 3(f).

Since the morphological features in the LMZs can easily be distorted by nonlinear propagating effects such as self-focusing and defocusing, we designed another experiment to avoid this issue. It is now well known that by adding a narrow slit on the top of the objective lens, the focal spot of the laser beam can be transversely expanded in glass due to the diffraction effect of the slit [Fig. 1(b)] [27]. Since the laser intensity will have a more homogeneous distribution in the transverse direction, self-focusing can be effectively mitigated, which results in only one well-defined focus in the longitudinal direction in the porous glass, as evidenced in Fig. 4. Here, the pulse energy was increased to 1.20 μJ, as the slit used in front of the objective lens inevitably blocked a large part of the laser beam and caused significant loss. The results obtained at scan velocities of 26, 8, 4.5, and 1.25 mm/s, which are presented in Figs. 4(a)–4(d), respectively, show no signature of nanograting formation. However, in Fig. 4(d), a boundary between the regions affected and unaffected by the laser irradiation can be

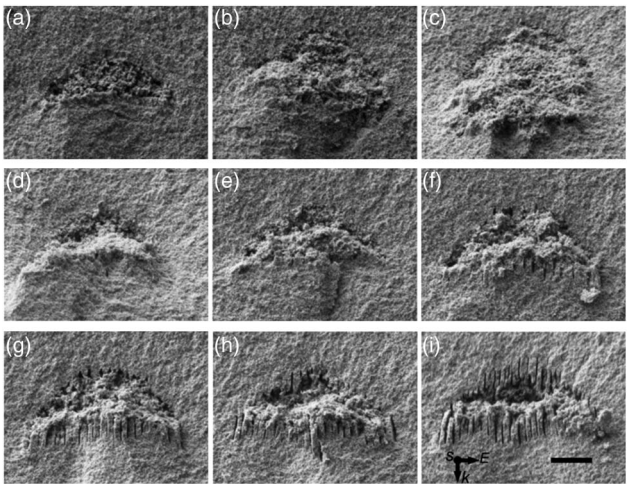


**Fig. 4.** Cross-sectional morphologies of nanogratings written with slit-beam shaping. Scan velocities in (a)–(i) are 26, 8, 4.5, 1.25, 0.50, 0.35, 0.10, 0.05, and 0.01 mm/s, respectively. Scale bar: 1 μm. The laser incident direction ($k$), polarization direction ($E$), and the writing direction ($S$) are indicated in the figure.

clearly seen. The next SEM image in Fig. 4(e) shows that at the interface, some periodically distributed nanovoids have been formed at a scan velocity of 0.5 mm/s. By further reducing the scan velocity to 0.35 mm/s, a few nanovoids develop into nanocracks, whereas the remaining nanovoids are almost unchanged [Fig. 4(f)]. At last, at a scan velocity of 0.01 mm/s, all the nanovoids develop into SWCs which leads to the formation of a perfect PNCA [Fig. 4(i)]. These results establish an important link between the formation of volume nanograting in glass and surface nanoripples on various substrates observed previously, as the interface created in bulk glass can play a similar role for surface plasma wave excitation [28,29].

The above observation provides crucial guidance for theoretical modeling. In all the simulations performed below, we ignore the influence of two consecutive pulses, because the plasma lifetime is much shorter than the interpulse period of our 250 kHz laser source [2,3]. First, we perform a finite difference time domain simulation to explain the SWC formation, as shown in Fig. 2. The nanovoid observed in Fig. 2(b) suggests that initially a spherical nanoplasma with a diameter of a few tens of nanometers was produced by multiphoton ionization in the glass. Thus, we assume that the nanoplasma has a diameter of 40 nm and a plasma density of $N_e = 5 \times 10^{20}$ cm$^{-3}$. This plasma density is chosen to best reproduce the experimental observations, because direct measurement of the plasma density in the volume of glass is difficult. Since the assumed size of the nanoplasma is much smaller than the laser wavelength, the laser field in our simulation is assumed to be a linearly polarized plane wave with a wavelength centered at 800 nm and a spectral width (FWHM) of ~30 nm. The relative dielectric constant of $SiO_2$ is assumed to be 2.1025. Using a Drude model, the relative dielectric constant in the laser field including the effect of $N_e$ can be derived as follows [29,30]:

$$\varepsilon = \varepsilon_m - \frac{N_e e^2}{\varepsilon_0 m^* m} \frac{1}{(\omega^2 + i w/\tau)}, \quad (1)$$

where is $\omega$ the incident light frequency in vacuum, $\tau$ is the Drude damping time of free electrons, and $\varepsilon_0$, $m$, $m^*$, and $e$ are the relative dielectric constant in vacuum, the electron mass, the optical effective mass of the carriers, and the electron charge, respectively. In reality, the Drude damping time varies as a function of the free electron density and temperature [31]. For simplicity, we chose a fixed Drude damping time of 10 fs in our simulation as in Ref. [32].

Figure 5(a) shows the simulated distribution of laser intensity around the spherical nanoplasma in the $x$–$z$ plane with $N_e = 5 \times 10^{20}$ cm$^{-3}$, $\varepsilon = 0.81945 + 0.03712i$. From Fig. 5(a), we can see a clear enhancement of the laser intensity inside the nanoplasma, as well as at its equator perpendicular to the incident electric-field vector. As explained in Ref. [33], the laser field inside the nanoplasma can be stronger than the incident field in an underdense nanoplasma ($0 < \mathrm{Re}(\varepsilon) < \varepsilon_m$), and a field enhancement occurs in the equatorial plane perpendicular to the electric field of light. This field enhancement will result in an asymmetric ablation around the nanoplasma, leading to formation of an elliptical nanoplasma.

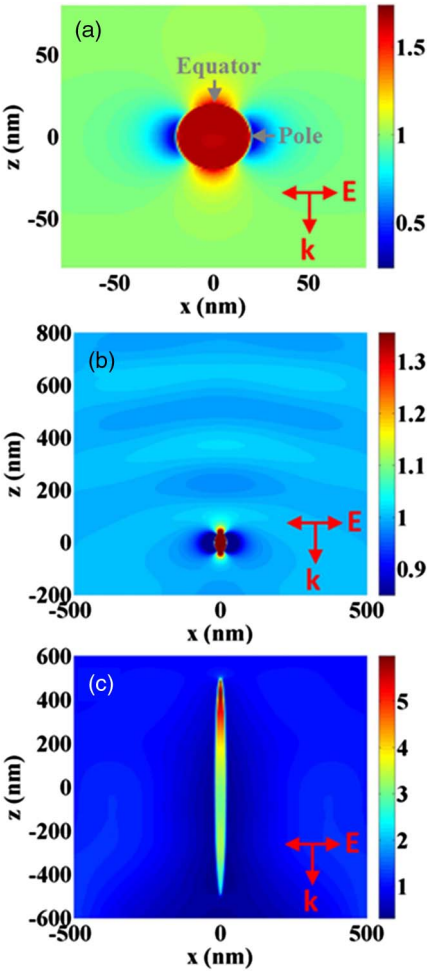


**Fig. 5.** Distribution of intensity of light in the $x$–$z$ plane near (a) a spherical-shaped nanoplasma ($R = 20$ nm) and (b), (c) two elliptical shaped nanoplasmas of different sizes. The sizes of elliptical nanoplasmas are $R_y = 20$ nm, $R_y = 40$ nm, and $R_z = 40$ nm in (b) and $R_x = 20$ nm, $R_y = 250$ nm, and $R_y = 250$ nm in (c). The laser incident direction ($k$) and the polarization direction ($E$) are indicated in the figures.

Next, we simulate the intensity distribution of light near an elliptical nanoplasma of $R_x = 20$ nm, $R_y = 40$ nm, $R_z = 40$ nm, as illustrated in Fig. 5(b). We observe that significant field enhancement has occurred at the tips of the elliptical nanoplasma [Fig. 5(b)], which promotes the growth of the nanoplasma along the main axis of the elliptical nanoplasma. Our further simulation shows that the field enhancement can also be observed for nanoplasma with larger ellipticities. This is evidenced in Fig. 5(c), which presents the optical intensity distribution in the vicinity of an elliptical nanoplasma of $R_x = 20$ nm, $R_y = 250$ nm, $R_z = 250$ nm. These results indicate that the field enhancement at the tips of the nanoplasma is responsible for the continuous growth of the SWC with an increasing number of laser pulses, which agrees well with our experimental observation in Fig. 2(e). The growth of a single SWC only ceases when it reaches the region where the laser peak intensity in the tight focal spot drops to a level below the ablation threshold.

At higher laser intensities far above the ablation threshold, a single nanovoid, as shown in Fig. 2, can no longer be formed. However, regardless of the focusing geometries, LMZs will be formed in glass due to melting and rapid resolidification. Surrounding the LMZs, there will always be the boundaries that become the interface between two kinds of materials with different optical properties. In some materials, the formed interfaces can provide suitable conditions for surface plasma excitation, which leads to the formation of an initial periodic nanovoid chain near the interface.

To model the plasma waves produced at the interface, the optical properties of the porous glass modified by the irradiation laser field should be considered. Indeed, the generation of high-density free electrons at the interface will lead to a significant change in the dielectric constant of the glass near the interface, which can be calculated using Eq. (1). In addition, similar to the excitation of a surface plasma wave with femtosecond laser pulses [28,34], plasma waves can also be excited at the interface, as illustrated in Fig. 6(a). Applying the boundary conditions to the field at the interface would result in the following expression for the plasma wave vector [35]:

$$k_{SPs} = k_0\sqrt{\frac{\varepsilon_m\varepsilon}{\varepsilon_m+\varepsilon}}, \tag{2}$$

provided that $\mathrm{Re}(\varepsilon) < -\varepsilon_m$. The electric field at the interface would be periodically enhanced with a spatial period of

$$d = \frac{\pi}{\mathrm{Re}(k_{SPs})}. \tag{3}$$

Figure 6(b) shows the period $d$ calculated as a function of $N_e$ within the region of $\mathrm{Re}(\varepsilon) < -\varepsilon_m$, which indicates that the minimum plasma density required for excitation of plasma waves is $N_e > 5\times10^{21}$ cm$^{-3}$. The calculated period is in the range of $d = 97$–$275$ nm, which is in good agreement with the nanograting period observed in the experiment. However, we would like to point out that the surface plasma waves excited at the interface do not necessarily directly induce the nanoscale ablation. Instead, the surface plasma waves can induce a periodic distribution of the defects formed near the interface, which facilitates subsequent ablation at the spots with a high density of defects. The periodically distributed nanovoids are evidenced by the experimental observation, as shown in Fig. 4(e). Afterward, each individual nanovoid can further develop into a SWC, eventually leading to the formation of the PNCA [Fig. 4(i)].

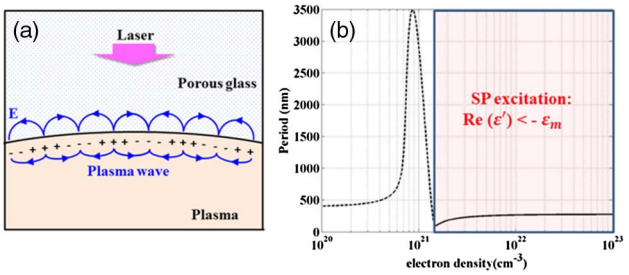


**Fig. 6.** (a) Concept of excitation of a surface plasma (SP) wave at an interface in the porous glass and (b) the calculated period of the surface plasma wave as a function of electron density. Excitation of surface plasma waves requires $\mathrm{Re}(\varepsilon) < -\varepsilon_m$.

One may notice that there could be a fundamental disadvantage of all models, speculating on the plasma effect, based on the fact that the plasma density cannot be constant over time in all experiments with laser pulses. Consequently, the plasma frequency can hardly be introduced, as it is a function of the rapidly varying plasma density. Here, we would like to provide an explanation of this contradiction as follows. It is well known that the response of transparent materials exposed to ultrafast laser pulses is highly nonlinear. Therefore, as the plasma density varies with time, the strongest modification in the material led by the plasma wave will occur within a brief moment when the strongest plasma wave is excited. For that brief moment, it can be a good approximation to assume a fixed frequency for the plasma wave, which has indeed been adopted in many previous investigations on the formation mechanism of femtosecond-laser-induced surface ripples [28,29].

In addition to plasma waves, Beresna *et al.* have recently proposed that self-organized exciton-polaritons could also mediate the formation of periodic nanostructures such as nanogratings or nanoripples [16]. The difficulty in applying this model to explain our observations is that the ablation induced by femtosecond laser irradiation actually occurs in a porous glass immersed in water. Indeed, it has been found that water plays a crucial role in the formation of nanogratings [36]. It is well known that plasma can be generated in both glass and water, but experimental evidence on exciton-polaritons has only been available for semiconductors. Therefore, we attempt to clarify whether exciton-polaritons could be generated in liquids such as water and how a model based on exciton-polaritons can be constructed to explain our observations in future investigations.

## 4. CONCLUSION

In conclusion, we have revealed the evolution of nanograting formation in a porous glass with an increasing number of irradiation pulses. We stress that nanograting formation is a multishot process, which involves accumulative modification of the volume of glass by irradiation of a femtosecond laser, and in turn the gradual shaping of the incident laser pulses when they are propagating in the evolving LMZ. Therefore, understanding how the morphology evolves in the volume of glass under multishot irradiation is vital. We observe that surface plasma waves excited at the interface can trigger the formation of nanogratings, which is further supported with our theoretical analyses. Our finding explains why the volume nanogratings formed in glasses share many similar features with femtosecond-laser-induced surface nanoripples, which also sheds light on the mechanism behind nanostructuring in transparent materials other than porous glass.

## FUNDING INFORMATION

National Basic Research Program of China (2014CB921300); National Science Foundation of China (NSFC) (61275205, 11104245, 61108015, 61008011, 11174305, 11104294, 61205209); European Research Council (ERC) under the Galatea Project (ERC-2012-StG-307442).

## ACKNOWLEDGMENT

Yves Bellouard acknowledges funding from the European Research Council (ERC) under the Galatea Project (ERC-2012-StG-307442).

†These authors contributed equally in this work.

## REFERENCES

1. A. Schiffrin, T. Paasch-Colberg, N. Karpowicz, V. Apalkov, D. Gerster, S. Mühlbrandt, M. Korbman, J. Reichert, M. Schultze, S. Holzner, J. V. Barth, R. Kienberger, R. Ernstorfer, V. S. Yakovlev, M. I. Stockman, and F. Krausz, "Optical-field-induced current in dielectrics," Nature **493**, 70–74 (2012).
2. R. R. Gattass and E. Mazur, "Femtosecond laser micromachining in transparent materials," Nat. Photonics **2**, 219–225 (2008).
3. K. Sugioka and Y. Cheng, "Ultrafast lasers—reliable tools for advanced materials processing," Light: Sci. Appl. **3**, e149 (2014).
4. P. G. Kazansky, H. Inouye, T. Mitsuyu, K. Miura, J. Qiu, and K. Hirao, "Anomalous anisotropic light scattering in Ge-doped silica glass," Phys. Rev. Lett. **82**, 2199–2202 (1999).
5. Y. Shimotsuma, P. G. Kazansky, J. Qiu, and K. Hirao, "Self-organized nano-gratings in glass irradiated by ultrashort light pulses," Phys. Rev. Lett. **91**, 247405 (2003).
6. V. R. Bhardwaj, E. Simova, P. P. Rajeev, C. Hnatovsky, R. S. Taylor, D. M. Rayner, and P. B. Corkum, "Optically produced arrays of planar nanostructures inside fused silica," Phys. Rev. Lett. **96**, 057404 (2006).
7. S. Kanehira, J. Si, J. Qiu, K. Fujita, and K. Hirao, "Periodic nanovoid structures via femtosecond laser irradiation," Nano Lett. **5**, 1591–1595 (2005).
8. Y. Liu, M. Shimizu, B. Zhu, Y. Dai, B. Qian, J. Qiu, Y. Shimotsuma, K. Miura, and K. Hirao, "Micromodification of element distribution in glass using femtosecond laser irradiation," Opt. Lett. **34**, 136–138 (2009).
9. P. G. Kazansky, W. Yang, E. Bricchi, J. Bovatsek, A. Arai, Y. Shimotsuma, K. Miura, and K. Hirao, "'Quill' writing with ultrashort light pulses in transparent materials," Appl. Phys. Lett. **90**, 151120 (2007).
10. W. Yang, P. G. Kazansky, and Y. P. Svirko, "Non-reciprocal ultrafast laser writing," Nat. Photonics **2**, 99–104 (2008).
11. W. Yang, P. G. Kazansky, Y. Shimotsuma, M. Sakakura, K. Miura, and K. Hirao, "Ultrashort-pulse laser calligraphy," Appl. Phys. Lett. **93**, 171109 (2008).
12. A. Vailionis, E. G. Gamaly, V. Mizeikis, W. Yang, A. V. Rode, and S. Juodkazis, "Evidence of superdense aluminium synthesized by ultrafast microexplosion," Nat. Commun. **2**, 445 (2011).
13. Y. Shimotsuma, M. Sakakura, P. G. Kazansky, M. Beresna, J. R. Qiu, K. Miura, and K. Hirao, "Ultrafast manipulation of self-assembled form birefringence in glass," Adv. Mater. **22**, 4039–4043 (2010).
14. M. Beresna, M. Gecevicius, P. G. Kazansky, and T. Gertus, "Radially polarized optical vortex converter created by femtosecond laser nanostructuring of glass," Appl. Phys. Lett. **98**, 201101 (2011).
15. Y. Liao, Y. Cheng, C. Liu, J. Song, F. He, Y. Shen, D. Chen, Z. Xu, Z. Fan, X. Wei, K. Sugioka, and K. Midorikawa, "Direct laser writing of sub-50 nm nanofluidic channels buried in glass for three-dimensional micro-nanofluidic integration," Lab Chip **13**, 1626–1631 (2013).
16. M. Beresna, M. Gecevičius, P. G. Kazansky, T. Taylor, and A. V. Kavokin, "Exciton mediated self-organization in glass driven by ultrashort light pulses," Appl. Phys. Lett. **101**, 053120 (2012).
17. R. Taylor, C. Hnatovsky, and E. Simova, "Applications of femtosecond laser induced self-organized planar nanocracks inside fused silica glass," Laser Photon. Rev. **2**, 26–46 (2008).
18. S. Richter, A. Plech, M. Steinert, M. Heinrich, S. Döring, F. Zimmermann, U. Peschel, E. B. Kley, A. Tünnermann, and S. Nolte, "On the fundamental structure of femtosecond laser-induced nanogratings," Laser Photon. Rev. **6**, 787–792 (2012).
19. Y. Liao, J. Song, E. Li, Y. Luo, Y. Shen, D. Chen, Y. Cheng, Z. Xu, K. Sugioka, and K. Midorikawa, "Rapid prototyping of three-dimensional microfluidic mixers in glass by femtosecond laser direct writing," Lab Chip **12**, 746–749 (2012).
20. Y. Liao, Y. Shen, L. Qiao, D. Chen, Y. Cheng, K. Sugioka, and K. Midorikawa, "Femtosecond laser nanostructuring in porous glass with sub-50 nm feature sizes," Opt. Lett. **38**, 187–189 (2013).
21. F. Liang, R. Vallée, and S. L. Chin, "Mechanism of nanograting formation on the surface of fused silica," Opt. Express **20**, 4389–4396 (2012).
22. P. Martin, S. Guizard, P. Daguzan, G. Petite, P. D'Oliveira, P. Meynadier, and M. Perdrix, "Subpicosecond study of carrier trapping dynamics in wide-band-gap crystals," Phys. Rev. B **55**, 5799 (1997).
23. S. Sakabe, M. Hashida, S. Tokita, S. Namba, and K. Okamuro, "Mechanism for self-formation of periodic grating structures on a metal surface by a femtosecond laser pulse," Phys. Rev. B **79**, 033409 (2009).
24. Y. Shimotsuma, K. Miura, and H. Kazuyuki, "Nanomodification of glass using fs laser," Int. J. Appl. Glass. Sci. **4**, 182–191 (2013).
25. M. Lancry, B. Poumellec, J. Canning, K. Cook, J.-C. Poulin, and F. Brisset, "Ultrafast nanoporous silica formation driven by femtosecond laser irradiation," Laser Photon. Rev. **7**, 953–962 (2013).
26. T. H. Elmer, "Porous and reconstructed glasses," in *Ceramics and Glasses*, S. J. Schneider, ed., Vol. **4** of Engineered Materials Handbook (ASM International, 1992), pp. 427–432.
27. Y. Cheng, K. Sugioka, K. Midorikawa, M. Masuda, K. Toyoda, M. Kawachi, and K. Shihoyama, "Control of the cross-sectional shape of a hollow microchannel embedded in photostructurable glass by use of a femtosecond laser," Opt. Lett. **28**, 55–57 (2003).
28. M. Huang and Z. Z. Xu, "Spontaneous scaling down of femtosecond laser-induced apertures towards the 10-nanometer level: the excitation of quasistatic surface plasmons," Laser Photon. Rev. **8**, 633–652 (2014).
29. G. Miyaji, K. F. Zhang, J. Fujita, and K. Miyazaki, "Nanostructuring of silicon surface with femtosecond-laser-induced near-field," J. Laser Micro/Nanoeng. **7**, 198–201 (2012).
30. C. V. Shank, R. Yen, and C. Hirlimann, "Time-resolved reflectivity measurements of femtosecond-optical-pulse-induced phase transitions in silicon," Phys. Rev. Lett. **50**, 454–457 (1983).
31. K. Sokolowski-Tinten and D. von der Linde, "Generation of dense electron-hole plasmas in silicon," Phys. Rev. B **61**, 2643–2650 (2000).
32. R. Buschlinger, S. Nolte, and U. Peschel, "Self-organized pattern formation in laser-induced multiphoton ionization," Phys. Rev. B **89**, 184306 (2014).
33. P. P. Rajeev, M. Gertsvolf, C. Hnatovsky, E. Simova, R. S. Taylor, P. B. Corkum, D. M. Rayner, and V. R. Bhardwaj, "Transient nanoplasmonics inside dielectrics," J. Phys. B **40**, S273–S282 (2007).
34. F. Garrelie, J. P. Colombier, F. Pigeon, S. Tonchev, N. Faure, M. Bounhalli, S. Reynaud, and O. Parriaux, "Evidence of surface plasmon resonance in ultrafast laser-induced ripples," Opt. Express **19**, 9035–9043 (2011).
35. A. M. Bonch-Bruevich, M. N. Libenson, V. S. Makin, and V. V. Trubaev, "Surface electromagnetic waves in optics," Opt. Eng. **31**, 718–730 (1992).
36. F. A. Umran, Y. Liao, M. M. Elias, K. Sugioka, R. Stoian, G. Cheng, and Y. Cheng, "Formation of nanogratings in a transparent material with tunable ionization property by femtosecond laser irradiation," Opt. Express **21**, 15259–15267 (2013).